
CONTEXT-AWARE VIDEO INSTANCE SEGMENTATION

Seunghun Lee*, Jiwan Seo*, Kiljoon Han, Minwoo Choi, and Sunghoon Im

Department of Electrical Engineering & Computer Science, DGIST, Daegu, Korea
{lsh5688, eccaron, kiljoon.h, subminu, sunghoonim}@dgist.ac.kr

ABSTRACT

In this paper, we introduce the Context-Aware Video Instance Segmentation (CAVIS), a novel framework designed to enhance instance association by integrating contextual information adjacent to each object. To efficiently extract and leverage this information, we propose the Context-Aware Instance Tracker (CAIT), which merges contextual data surrounding the instances with the core instance features to improve tracking accuracy. Additionally, we introduce the Prototypical Cross-frame Contrastive (PCC) loss, which ensures consistency in object-level features across frames, thereby significantly enhancing instance matching accuracy. CAVIS demonstrates superior performance over state-of-the-art methods on all benchmark datasets in video instance segmentation (VIS) and video panoptic segmentation (VPS). Notably, our method excels on the OVIS dataset, which is known for its particularly challenging videos. Project page: [this https URL](#)

1 INTRODUCTION

Video Instance Segmentation (VIS) is a crucial task that involves segmenting and identifying individual objects within video sequences, applicable in a variety of fields including video understanding, autonomous driving, and video editing (Yang et al., 2019). VIS has seen considerable advancements, with developments in both online methods (Yang et al., 2019; Cao et al., 2020; Yang et al., 2021b; Huang et al., 2022; Wu et al., 2022c; Ying et al., 2023; Kim et al., 2024), which process videos frame-by-frame to adapt in real-time, and offline methods (Wang et al., 2021; Hwang et al., 2021; Wu et al., 2022b; Cheng et al., 2021a; Heo et al., 2022), which analyze entire videos to understand inter-frame dependencies thoroughly.

Recent advances have brought robust query-based segmentation architectures (Cheng et al., 2021b; 2022), designed to detect instance centers and cluster pixels into instance-specific groups within images. These modern VIS approaches increasingly employ instance center associations across frames to improve tracking accuracy. Techniques such as contrastive learning (Wu et al., 2022c; Ying et al., 2023) and transformer-based trackers (Heo et al., 2023; Zhang et al., 2023a) leverage the similarities between instance centers for consistent identification of objects across frames. However, challenges persist in scenarios with significant occlusions or when multiple similar objects are present, leading to potential tracking inaccuracies as shown in the top row of Fig. 1. While some strategies (Heo et al., 2022; 2023) attempt to use instance features for tracking across segments or entire videos, difficulties remain.

To address this issue, we propose Context-Aware Video Instance Segmentation (CAVIS), a novel framework designed to improve object identification by incorporating contextual information surrounding each instance into the tracking process. This approach draws from insights in neuroscience and cognitive science (Bar, 2004; Oliva & Torralba, 2007), emphasizing the importance of contextual cues in human perception for deciphering complex scenes and resolving visual ambiguities. An example of the practical application of this principle is shown in Fig. 1, where recognizing a person is riding a bicycle, rather than just identifying the bicycle, greatly enhances the accuracy of object identification.

To achieve this, we design the Context-Aware Instance Tracker (CAIT), featuring advanced modules for extracting and matching context-aware instance features. The context-aware instance feature extractor combines the contextual information at the object’s boundary with the core features of

*These authors contribute equally to this work.

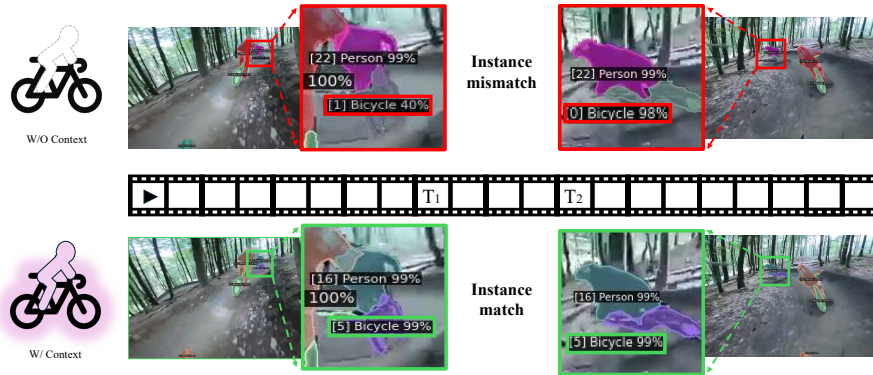


Figure 1: **Importance of contextual information.** Comparative results showing the state-of-the-art model (Zhang et al., 2023b) (Top) and CAVIS (Bottom). The frame on the left precedes the right by four frames, during which an occlusion takes place. The standard model, lacking contextual data, fails to consistently track the same bicycle post-occlusion, while CAVIS effectively maintains accurate instance tracking.

each instance. Then, we incorporate these context-aware instance features into a transformer-based tracking architecture (Wu et al., 2022b; Heo et al., 2023; Zhang et al., 2023a), enhanced by our novel context-aware cross-attention mechanism. This adjustment allows for the precise utilization of detailed contextual nuances within each scene.

Furthermore, we introduce the Prototypical Cross-frame Contrastive (PCC) loss to ensure feature consistency across frames. Utilizing a query-based segmenter, PCC loss correlates each pixel with an object by comparing core instance features against pixel embeddings, enhancing regional consistency within frames and establishing an intra-frame constraint reflective of the feature map’s similarity. This method crucially maps inter-frame pixel relationships, bolstering object association—a vital aspect for contrastive learning that differentiates similar from dissimilar objects across frames. However, maintaining individual pixel consistency is memory-intensive. To address this, PCC loss strategically constructs instance-wise prototypes to maintain frame-to-frame consistency, thereby boosting training efficiency and ensuring robust performance in dynamic environments.

Our extensive testing shows that CAVIS significantly outperforms existing state-of-the-art methods across major video segmentation benchmarks, including YTVIS19 (Yang et al., 2019), YTVIS21 (Yang et al., 2021a), OVIS (Qi et al., 2022), and VIPSeg (Miao et al., 2021), particularly excelling on OVIS dataset that include complex video sequences. Our contributions to the field are manifold and can be summarized as follows:

1. We present Context-Aware Instance Tracker (CAIT), a novel framework designed to extract context-aware instance features and utilize them for enhanced instance matching.
2. We propose a Prototypical Cross-frame Contrastive (PCC) loss that enhances the learning of instance matching by ensuring consistency in object-level features across frames.
3. Our model demonstrates robustness in challenging videos environments, establishing state-of-the-art performance in Video Instance Segmentation and Video Panoptic Segmentation.

2 RELATED WORKS

Video Instance Segmentation. VIS methods learn to associate features frame-to-frame based on instance segmentation architectures. The pioneering MaskTrack R-CNN (Yang et al., 2019) integrates a tracking head into Mask R-CNN (He et al., 2017), utilizing heuristic cues for instance association. Following advancements include SipMask (Cao et al., 2020) and CrossVIS (Yang et al., 2021b), which enhance temporal links through cross-frame learning. IDOL(Wu et al., 2022c) a contrastive learning approach with query-based architectures (Zhu et al., 2020), boosting online method performance. Conversely, offline approaches like VisTR (Wang et al., 2021) and Seqformer (Wu et al., 2022b) use the entire video for mask trajectory predictions, with VisTR applying DETR (Carion et al., 2020) at the clip level and Seqformer aggregating temporal information via inter-frame queries. Innovations

like IFC (Hwang et al., 2021) and TeViT (Yang et al., 2022) improve efficiency by adjusting attention mechanisms within transformer architectures.

Advancements in Query-based Networks. Strong query-based segmentation networks have become prevalent in current VIS methods, with many relying on Mask2Former (Cheng et al., 2022) as their foundation. MinVIS (Huang et al., 2022) achieves tracking through simple post-processing based on cosine similarity between object features, without video learning. VITA (Heo et al., 2022) temporally associates frame-level queries to find instance prototypes within a video. GenVIS (Heo et al., 2023) adopts object association approach of VITA and designs a tracking network at the sub-clip level. Inspired by SimCLR (Chen et al., 2020), CTVIS (Ying et al., 2023) utilizes contrastive learning with a larger number of frames for comprehensive frame association. DVIS (Zhang et al., 2023a) introduces a decoupled framework for VIS, dividing it into segmentation, tracking, and refinement tasks, thereby enabling efficient and effective learning.

Object Tracking with Additional Cues. Tracking methodologies have been developed across various domains, including video object segmentation (VOS) (Xu et al., 2018; Oh et al., 2019; Cheng et al., 2021c), multiple object tracking (MOT) (Milan et al., 2016; Bergmann et al., 2019; Zhou et al., 2020; Zhang et al., 2021), and VIS. Despite advancements, many challenging cases persist, prompting research into object association with supplementary data. Early approaches leverage spatial-temporal information such as geometric relation between adjacent frames (Tang et al., 2017) and aggregated object features of previous frames (Xu et al., 2019). BeyondPixel (Sharma et al., 2018) improves inter-frame object matching by proposing a new cost that captures 3D pose and shape based on monocular geometry. BATMAN (Yu et al., 2022) combines optical flow and object query features to encode motion and appearance information into bilateral space. (Choudhuri et al., 2023) introduces a context-aware relative query which reflects global and local context by aggregating multi-level image features from consecutive frames.

3 PRELIMINARY

This section offers a concise introduction to the fundamentals of a query-based instance segmentation pipeline and outlines a VIS approach that incorporates contrastive learning (Wu et al., 2022c; Li et al., 2023b; Ying et al., 2023; Li et al., 2023c).

3.1 QUERY-BASED INSTANCE SEGMENTATION

Modern VIS methods adopt a query-based instance segmentation pipeline (Cheng et al., 2021b; 2022), including three main components: a backbone encoder, a pixel decoder, and a transformer decoder. The backbone encoder and pixel decoder are responsible for extracting multi-scale feature maps from the input image. The transformer decoder employs object queries—sequences of latent vectors—as initial guesses for object centers and utilizes these features to generate object-level features. These queries undergo refinement through multiple transformer blocks via a cross-attention mechanism between the object queries and the feature maps. The refined instance features are then used for classification and segmentation tasks through respective prediction heads. Typically, the number of object queries, N , exceeds the actual number of objects, N_{GT} , present in the image. Traditionally, the process involves finding a permutation of N elements, $\sigma \in \mathfrak{S}_N$, that optimally assigns the prediction set $\{\hat{y}_i\}_{i=1}^N$ to maximize total similarity to the ground truth (GT) set $\{y_i\}_{i=1}^{N_{GT}}$. This is achieved by minimizing a pair-wise matching cost $\mathcal{L}_{\text{Match}}$, as defined in (Cheng et al., 2021a):

$$\hat{\sigma} = \arg \min_{\sigma \in \mathfrak{S}_N} \sum_{k=1}^{N_{GT}} \mathcal{L}_{\text{Match}}(y_k, \hat{y}_{\sigma(k)}). \quad (1)$$

The network is trained with an objective function, $\mathcal{L}_{\text{Inst}}$, which consists of a categorical loss (\mathcal{L}_{Cls}), a binary cross-entropy loss for masks (\mathcal{L}_{Bce}), and a dice loss ($\mathcal{L}_{\text{Dice}}$) with the weights λ_{Cls} , λ_{Bce} , and λ_{Dice} balancing the contributions of each loss component as follows:

$$\mathcal{L}_{\text{Inst}} = \lambda_{\text{Cls}} \mathcal{L}_{\text{Cls}} + \lambda_{\text{Bce}} \mathcal{L}_{\text{Bce}} + \lambda_{\text{Dice}} \mathcal{L}_{\text{Dice}}. \quad (2)$$

The loss is used to train VIS framework with the frame-wise matching relation $\hat{\sigma}^t$ as follows:

$$\mathcal{L}_{\text{VIS}} = \sum_{t=1}^T \sum_{n=1}^{N_{GT}} \mathcal{L}_{\text{Inst}}(y_n^t, \hat{y}_{\hat{\sigma}^t(n)}^t). \quad (3)$$

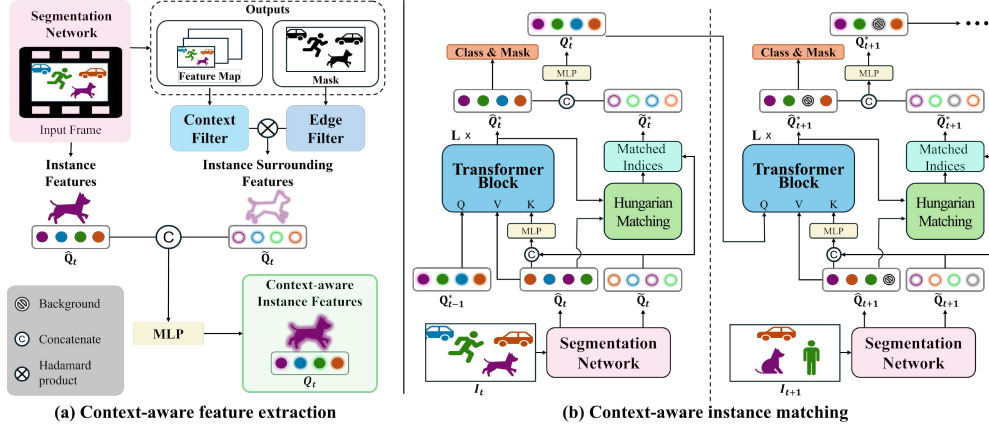


Figure 2: **Overview of CAVIS.** (a) The extraction of **context-aware instance features** from the output of an instance segmentation network. (b) CAVIS pipeline through **context-aware instance matching**. This includes the organization of the surrounding instance features \hat{Q}_t , facilitated by Hungarian matching between the ordered instance features \hat{Q}_t^* and unordered instance features \hat{Q}_t .

3.2 CONTRASTIVE LEARNING FOR VIS

In query-based architectures, the order of instance features effectively serves as the identity of each object. By aligning the sequence of instance features across frames, we can facilitate object tracking. Since instance features represent specific objects, inter-frame feature association is used for this alignment. To enhance the robustness of instance features for matching objects between frames, the following contrastive loss is integrated within the VIS framework (Wu et al., 2022c):

$$\begin{aligned} \mathcal{L}_{\text{Emb}}(v_t) &= -\log \frac{\sum_{k^+ \in \mathbf{K}_{v_t}^+} \exp(v_t \cdot k^+)}{\sum_{k^+ \in \mathbf{K}_{v_t}^+} \exp(v_t \cdot k^+) + \sum_{k^- \in \mathbf{K}_{v_t}^-} \exp(v_t \cdot k^-)}, \\ &= \log \left[1 + \sum_{k^+ \in \mathbf{K}_{v_t}^+} \sum_{k^- \in \mathbf{K}_{v_t}^-} \exp(v_t \cdot k^- - v_t \cdot k^+) \right], \quad \forall t \in \{1, \dots, T\}, \end{aligned} \quad (4)$$

where $\mathbf{K}_{v_t}^+$ represents the sets of positive embeddings corresponding to the same object as v_t from frames other than the t -th frame, while $\mathbf{K}_{v_t}^-$ includes negative embeddings featuring characteristics of objects different from that of v_t .

4 METHOD

This section describes our Context-Aware Video Instance Segmentation (CAVIS) whose overall pipeline is illustrated in Fig. 2. Our CAVIS consists of two key components: Context-Aware Instance Tracker (CAIT) and Prototypical Cross-frame Contrastive (PCC) loss, which are detailed in Sec. 4.1 and Sec. 4.2, respectively. We describe the training losses for each network in Sec. 4.3.

4.1 CONTEXT-AWARE INSTANCE TRACKER

4.1.1 CONTEXT-AWARE FEATURE EXTRACTION

Following the method outlined in previous VIS studies (Huang et al., 2022; Heo et al., 2022; 2023; Ying et al., 2023; Zhang et al., 2023a), we employ Mask2Former (Cheng et al., 2022) as our segmentation network \mathcal{S} . This framework ingests a series of input frames $\{I_t\}_{t=1}^T$, with T denoting the total number of frames. It extracts feature maps F , identifies instance features \hat{Q} , and computes

both classification scores O and generates segmentation masks M as follows:

$$\begin{aligned} \left\{ F_t, \hat{Q}_t, O_t, M_t \right\}_{t=1}^T &= \mathcal{S} \left(\{ I_t \}_{t=1}^T \right), \\ F_t \in \mathbb{R}^{H \times W \times C}, \hat{Q}_t \in \mathbb{R}^{N \times C}, O_t \in \mathbb{R}^{N \times K}, M_t \in \mathbb{R}^{N \times H \times W}, \end{aligned} \quad (5)$$

where H , W , and C denote the height, width, and channel dimensions of the feature maps, respectively. N indicates the maximum number of detectable objects in a single frame, and K signifies the number of object classes. We then extract the instance surrounding features $\hat{Q}_t \in \mathbb{R}^{N \times C}$ capturing data around the object’s boundaries essential for detailed context analysis as follows:

$$\tilde{Q}_t^n = \frac{\sum_{h=1}^H \sum_{w=1}^W \bar{F}_t^{\{h,w\}} * \mathbb{1} \left(\hat{M}_t^{\{n,h,w\}} > 0 \right)}{\sum_{h=1}^H \sum_{w=1}^W \mathbb{1} \left(\hat{M}_t^{\{n,h,w\}} > 0 \right)}, \quad \forall n = \{1, \dots, N\}, \quad (6)$$

$$\text{where } \bar{F} = \text{Avg}(F), \hat{M} = \text{Lap}(M),$$

where $\text{Avg}(\cdot)$ denotes an average filtering process, $\text{Lap}(\cdot)$ signifies the application of a Laplacian filter, and $\mathbb{1}(\cdot)$ is the indicator function that tests for the presence of the object within the filtered mask. We employ the average filter specifically configured with a 9×9 kernel size.

Finally, we combine the core and surrounding features to further enhance instance representations. The context-aware instance feature $Q_t^n \in \mathbb{R}^C$ is generated by concatenating the core instance feature \hat{Q}_t^n and the instance surrounding feature \tilde{Q}_t^n , and subsequently processing this combined feature through a multi-layer perceptron (MLP) as follows:

$$Q_t^n = \text{MLP} \left(\text{Concat} \left(\hat{Q}_t^n, \tilde{Q}_t^n \right) \right), \quad \forall n = \{1, \dots, N\}. \quad (7)$$

The MLP is structured with three linear layers, each followed by a ReLU activation function. To promote the learning of discriminative context-aware instance features, we implement a contrastive loss specifically for these features. The context-aware contrastive loss, denoted as \mathcal{L}_{CTX} , leverages the established contrastive loss framework \mathcal{L}_{Emb} detailed in Eq. (4) as follows:

$$\mathcal{L}_{\text{CTX}} = \sum_{t=1}^T \sum_{n=1}^{N_{GT}} \mathcal{L}_{\text{Emb}} \left(Q_t^{\hat{\sigma}^t(n)} \right), \quad (8)$$

where $\hat{\sigma}^t$ is a frame-wise matching relation as described in Eq. (1). This design enhances our ability to identify and track the same instances across the entire video. By not solely relying on instance centers, and instead utilizing context-aware instance embeddings, we can more accurately recognize instances throughout the video sequence.

4.1.2 CONTEXT-AWARE INSTANCE MATCHING

We introduce our context-aware tracking network \mathcal{T} , which employs a transformer-based tracking network (Heo et al., 2023; Zhang et al., 2023a) to learn associations across adjacent frames. The network comprises six transformer blocks, each featuring cross-attention, self-attention, and feed-forward layers. The conventional cross-attention mechanism, denoted as $\text{Attn}(Q, K, V)$, traditionally aligns the current unordered instance features, \hat{Q}_t , (serving as both the key and value), with the ordered instance features from the previous frame, \hat{Q}_{t-1}^* , (used as the query). To enhance accuracy, our model employs context-aware instance features, Q_{t-1}^* and Q_t , as the query and key, respectively while we still use the instance features \hat{Q}_t as value. This modification leads to a context-aware cross-attention mechanism, formulated as:

$$\text{Attn}(Q_{t-1}^*, Q_t, \hat{Q}_t) = \text{softmax} \left(\frac{Q_{t-1}^* \cdot (Q_t)^T}{\sqrt{C}} \right) \hat{Q}_t, \quad (9)$$

where C is the channel dimensions of the feature maps. The aligned context-aware instance features Q_t^* is built by concatenating the aligned instance features \hat{Q}_t^* and the aligned instance surrounding features \tilde{Q}_t^* same as in Eq. (7). We obtain the aligned instance surrounding features \tilde{Q}_t^* by using Hungarian matching algorithm (Kuhn, 1955) on cosine similarity between \hat{Q}_t and \hat{Q}_t^* as follows:

$$\tilde{Q}_t^{*\sigma_H(n)} = \tilde{Q}_t^n, \quad \forall n = \{1, \dots, N\}, \quad \text{where } \sigma_H = \text{Hungarian}(\hat{Q}_t^*, \hat{Q}_t), \quad \sigma_H \in \mathbb{R}^N. \quad (10)$$

This process is similarly applied to the aligned context-aware features Q_{t-1}^* for the previous frame.

4.2 PROTOTYPICAL CROSS-FRAME CONTRASTIVE LOSS

Our method employs a query-based segmenter to assess each pixel’s relationship to an object by comparing core instance features, $\hat{Q}_t^n \in \mathbb{R}^C$, with corresponding pixel embeddings, $F_t^{\{h,w\}} \in \mathbb{R}^C$. This process ensures consistent feature representation within object-containing regions and introduces an intra-frame constraint that reflects similarity within the feature map. By examining the inter-frame relationships of pixel embeddings, our method improves object association, essential for contrastive learning methods that strive to differentiate between similar and dissimilar objects across frames.

Given the memory-intensive nature of maintaining individual pixel consistency, we introduce Prototypical Cross-frame Contrastive (PCC) loss. This loss \mathcal{L}_{PCC} maintains frame-to-frame consistency of pixel embeddings for each instance feature by constructing instance-wise prototypes from predicted masks, defined as follows:

$$\mathcal{L}_{\text{PCC}} = \sum_{t=1}^T \sum_{n=1}^{N_{GT}} \mathcal{L}_{\text{Emb}} \left(\eta_t^{\hat{\sigma}^t(n)} \right), \quad \eta_t^n = \frac{\sum_{h=1}^H \sum_{w=1}^W F_t^{\{h,w\}} * \mathbb{1} \left(M_t^{\{h,w\}} == 1 \right)}{\sum_{h=1}^H \sum_{w=1}^W \mathbb{1} \left(M_t^{\{h,w\}} == 1 \right)}. \quad (11)$$

4.3 TRAINING LOSS

To train the segmentation network \mathcal{S} , we implement an objective function that incorporates the standard video instance segmentation loss \mathcal{L}_{VIS} in Eq. (3), context-aware contrastive loss \mathcal{L}_{CTX} in Eq. (8) and Prototypical Cross-frame Contrastive (PCC) loss in Eq. (11) as follows:

$$\mathcal{L}_{\mathcal{S}} = \mathcal{L}_{\text{VIS}} + \lambda_{\text{CTX}} \mathcal{L}_{\text{CTX}} + \lambda_{\text{PCC}} \mathcal{L}_{\text{PCC}}, \quad (12)$$

where λ_{CTX} and λ_{PCC} are the weights assigned to balance these losses.

To train the tracking network \mathcal{T} , we calculate the matching cost only for objects that appear for the first time to ensure consistent video-level matching pairs, as implemented in prior work (Zhang et al., 2023a). The objective function $\mathcal{L}_{\mathcal{T}}$ incorporating the matching relation $\hat{\sigma}_{\text{con}}$ is defined as follows:

$$\mathcal{L}_{\mathcal{T}} = \sum_{t=1}^T \sum_{n=1}^{N_{GT}} \mathcal{L}_{\text{Inst}} \left(y_n^t, \hat{y}_{\hat{\sigma}_{\text{con}}^t(n)}^t \right), \quad \hat{\sigma}_{\text{con}} = \arg \min_{\sigma \in \mathfrak{S}_N} \sum_{k=1}^{N_{GT}} \mathcal{L}_{\text{Match}} \left(y_k^{f(k)}, \hat{y}_{\sigma(k)}^{f(k)} \right), \quad (13)$$

where $f(k)$ denotes the frame in which the k -th instance first appears.

5 EXPERIMENTS

We evaluate CAVIS on two major tasks: video instance segmentation (VIS) and video panoptic segmentation (VPS) on four benchmark datasets recognized for their challenges and prevalence in the research community: YouTubeVIS-2019 (Yang et al., 2019), YouTubeVIS-21 (Yang et al., 2021a), OVIS (Qi et al., 2022), and VIPSeg (Miao et al., 2021). For VIS, performance metrics include average precision (AP) and average recall (AR) as established in previous studies (Yang et al., 2019). In the realm of VPS (Kim et al., 2020), we further examine our model’s capabilities using the Segmentation and Tracking Quality (STQ) metric, and the Video Panoptic Quality (VPQ) metric.

5.1 IMPLEMENTATION DETAILS

We employ Mask2Former (Cheng et al., 2022) as our segmentation network, utilizing three distinct backbone encoders: ResNet-50 (He et al., 2016), Swin-L (Liu et al., 2021), and ViT-L (Dosovitskiy et al., 2021). The ResNet-50 and Swin-L backbones are initialized with parameters pre-trained on the COCO dataset (Lin et al., 2014), while the ViT-L backbone uses initialization parameters from DINOv2 (Oquab et al., 2023). Additionally, for the ViT-L backbone, we employ a memory-efficient version of ViT-Adapter (Chen et al., 2022), aligning with recent advancements in network efficiency (Zhang et al., 2023b). Further details are described in Sec. A.2.2.

5.2 COMPARISON TO STATE-OF-THE-ART METHODS

Video Instance Segmentation (VIS). We benchmark CAVIS against leading methods on three established VIS datasets, as detailed in Tab. 1. CAVIS sets a new state-of-the-art, outperforming

Table 1: Comparisons on the validation sets of YouTube-VIS 2019, 2021, and OVIS datasets. The best and second-best scores are highlighted in **red** and **blue**, respectively. † denotes the model trained with the temporal refiner (Zhang et al., 2023a). Rows in cyan indicate comparisons with a top-performing model.

Methods		OVIS					YTVIS19					YTVIS21				
		AP	AP ₅₀	AP ₇₅	AR ₁	AR ₁₀	AP	AP ₅₀	AP ₇₅	AR ₁	AR ₁₀	AP	AP ₅₀	AP ₇₅	AR ₁	AR ₁₀
ResNet-50	MaskTrack R-CNN (Yang et al., 2019)	10.8	25.3	8.5	7.9	14.9	30.3	51.1	32.6	31.0	35.5	28.6	48.9	29.6	26.5	33.8
	SipMask (Cao et al., 2020)	10.2	24.7	7.8	7.9	15.8	33.7	54.1	35.8	35.4	40.1	31.7	52.5	34.0	30.8	37.8
	IFC (Hwang et al., 2021)	13.1	27.8	11.6	9.4	23.9	41.2	65.1	44.6	42.3	49.6	35.2	55.9	37.7	32.6	42.9
	CrossVIS (Yang et al., 2021b)	14.9	32.7	12.1	10.3	19.8	36.3	56.8	38.9	35.6	40.7	34.2	54.4	37.9	30.4	38.2
	EfficientVIS (Wu et al., 2022a)	-	-	-	-	-	37.9	59.7	43.0	40.3	46.6	34.0	57.5	37.3	33.8	42.5
	SeqFormer (Wu et al., 2022b)	15.1	31.9	13.8	10.4	27.1	47.4	69.8	51.8	45.5	54.8	40.5	62.4	43.7	36.1	48.1
	VISOLO (Han et al., 2022)	15.3	31.0	13.8	11.1	21.7	38.6	56.3	43.7	35.7	42.5	36.9	54.7	40.2	30.6	40.9
	Mask2Former-VIS (Cheng et al., 2021a)	17.3	37.3	15.1	10.5	23.5	46.4	68.0	50.0	-	-	40.6	60.9	41.8	-	-
	VITA (Heo et al., 2022)	19.6	41.2	17.4	11.7	26.0	49.8	72.6	54.5	49.4	61.0	45.7	67.4	49.5	40.9	53.6
	MinVIS (Huang et al., 2022)	25.0	45.5	24.0	13.9	29.7	47.4	69.0	52.1	45.7	55.7	44.2	66.0	48.1	39.2	51.7
	IDOL (Wu et al., 2022c)	28.2	51.0	28.0	14.5	38.6	49.5	74.0	52.9	47.7	58.7	43.9	68.0	49.6	38.0	50.9
	DVIS (Zhang et al., 2023a)	30.2	55.0	30.5	14.5	37.3	51.2	73.8	57.1	47.2	59.3	46.4	68.4	49.6	39.7	53.5
	TCOVIS (Li et al., 2023a)	35.3	60.7	36.6	15.7	39.5	52.3	73.5	57.6	49.8	60.2	49.5	71.2	53.8	41.3	55.9
	CTVIS (Ying et al., 2023)	35.5	60.8	34.9	16.1	41.9	55.1	78.2	59.1	51.9	63.2	50.1	73.7	54.7	41.8	59.5
	GenVIS (Heo et al., 2023)	35.8	60.8	36.2	16.3	39.6	50.0	71.5	54.6	49.5	59.7	47.1	67.5	51.5	41.6	54.7
Ours	37.6	63.4	38.2	16.5	43.5	55.7	78.3	61.7	51.5	63.3	50.5	74.1	54.9	42.6	58.5	
Swin-L	SeqFormer (Wu et al., 2022b)	-	-	-	-	-	59.3	82.1	66.4	51.7	64.4	51.8	74.6	58.2	42.8	58.1
	Mask2Former-VIS (Cheng et al., 2021a)	25.8	46.5	24.4	13.7	32.2	60.4	84.4	67.0	-	-	52.6	76.4	57.2	-	-
	VITA (Heo et al., 2022)	27.7	51.9	24.9	14.9	33.0	63.0	86.9	67.9	56.3	68.1	57.5	80.6	61.0	47.7	62.6
	MinVIS (Huang et al., 2022)	39.4	61.5	41.3	18.1	43.3	61.6	83.3	68.6	54.8	66.6	55.3	76.6	62.0	45.9	60.8
	IDOL (Wu et al., 2022c)	40.0	63.1	40.5	17.6	46.4	64.3	87.5	71.0	55.6	69.1	56.1	80.8	63.5	45.0	60.1
	GenVIS (Heo et al., 2023)	45.2	69.1	48.4	19.1	48.6	64.0	84.9	68.3	56.1	69.4	59.6	80.9	65.8	48.7	65.0
	DVIS (Zhang et al., 2023a)	45.9	71.1	48.3	18.5	51.5	63.9	87.2	70.4	56.2	69.0	58.7	80.4	66.6	47.5	64.6
	TCOVIS (Li et al., 2023a)	46.7	70.9	49.5	19.1	50.8	64.1	86.6	69.5	55.8	69.0	61.3	82.9	68.0	48.6	65.1
	CTVIS (Ying et al., 2023)	46.9	71.5	47.5	19.1	52.1	65.6	87.7	72.2	56.5	70.4	61.2	84.0	68.8	48.0	65.8
	Ours	48.6	74.0	52.5	19.5	53.3	66.0	89.5	73.3	56.8	71.4	61.1	84.1	69.2	48.2	66.3
ViT-L	MinVIS (Huang et al., 2022)	42.9	65.7	45.4	19.8	46.5	65.6	85.4	72.7	57.5	70.6	59.2	79.9	66.7	47.8	64.1
	DVIS++ (Zhang et al., 2023b)	49.6	72.5	55.0	20.8	54.6	67.7	88.8	75.3	57.9	73.7	62.3	82.7	70.2	49.5	68.0
	Ours	53.2	75.9	59.1	20.9	58.2	68.9	89.3	76.2	58.3	73.6	64.6	85.6	72.5	49.5	69.3
	DVIS++† (Zhang et al., 2023b)	53.4	78.9	58.5	21.1	58.7	68.3	90.3	76.1	57.8	73.4	63.9	86.7	71.5	48.8	69.5
	Ours†	57.1	82.6	63.5	21.2	61.8	69.4	90.9	77.2	58.3	74.7	65.3	87.3	73.2	49.7	70.3

the previous top model, DVIS++, by margins of 1.1, 1.4, and 3.7 average precision (AP) points on YouTube-VIS2019, YouTube-VIS2021, and OVIS, respectively. Particularly noteworthy is CAVIS’s performance on the OVIS dataset, where it significantly outstrips all competitors. This dataset is renowned for its diversity and the complexity of its video sequences. Fig. 3 illustrates how our model proficiently tracks objects even in scenarios marked by severe occlusion. This capability underscores the strength of our context-aware video learning approach, which effectively leverages information from surrounding objects for accurate instance matching, even under severe occlusion.

Video Panoptic Segmentation (VPS). In the realm of VPS, CAVIS also achieves the best performance on the VIPSeg dataset as shown in Tab. 2. For the ResNet-50 backbone, it achieves 45.3 in both Video Panoptic Quality (VPQ) and Segmentation and Tracking Quality (STQ). For the ViT-L backbone, the figures reach 58.5 VPQ and 56.1 STQ, demonstrating substantial advancements. Specifically, our model shows significant gains in VPQTh—which assesses performance on ‘thing’ classes—with increases of 3.0 and 1.9 for ResNet-50 and ViT-L backbones, respectively, over the previous best models. These improvements highlight the versatility of our context-aware object matching strategy across various video segmentation tasks.

5.3 ABLATION STUDY

We conduct ablation studies on the OVIS dataset (Qi et al., 2022) with the ResNet-50 (He et al., 2016) backbone over 40k training iterations, detailed in Tab. 3. For these tests, we sample two frames from each input video for experiments listed in Tab. 3-(a), (b), and (d). To evaluate the segmentation network across these setups in Tab. 3-(a-d), we employ the minimal post-processing method proposed by MinVIS (Huang et al., 2022).

Ablation study on technical contributions of CAVIS. We conduct a series of experiments to demonstrate the effectiveness of our key components: the context-aware instance tracker (CAIT) and prototypical cross-frame contrastive (PCC) loss. The results, shown in Tab. 3-(a) for the segmentation network and Tab. 3-(e) for the tracking network, demonstrate significant performance enhancements.

Tab. 3-(a) includes six experiments (i- vi), where experiment (i) present our baseline performance of retraining MinVIS (Huang et al., 2022) to match our settings. Experiments (i- iii) show that implementing contrastive learning, whether with standard or context-aware instance features, leads to

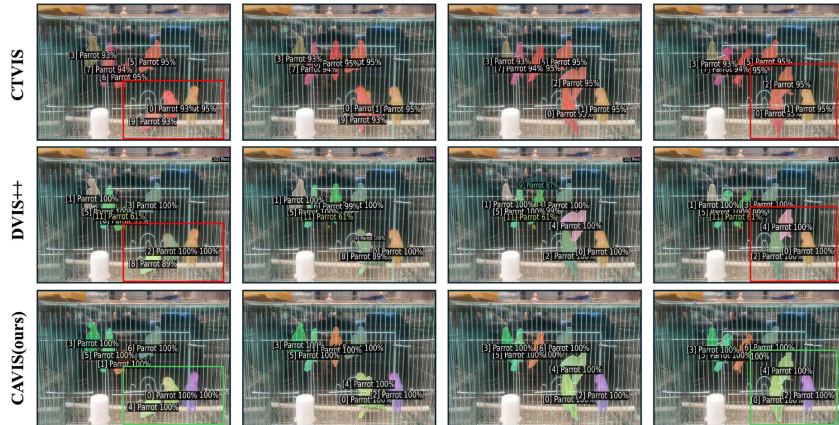


Figure 3: Qualitative comparisons of CAVIS (ours) against state-of-the-art methods: CTVIS (Ying et al., 2023) and DVIS++ (Zhang et al., 2023b) on the OVIS dataset.

Table 2: Comparison on VIPSeg validation sets. ‘Th’ and ‘St’ denote ‘things’ and ‘stuff’ classes.

Method	ResNet-50				ViT-L			
	VPQ	VPQ Th	VPQ St	STQ	VPQ	VPQ Th	VPQ St	STQ
VPSNet-SiamTrack(Woo et al., 2021)	17.2	17.3	17.3	21.1	-	-	-	-
VIP-Deeplab(Qiao et al., 2021)	16.0	12.3	18.2	22.0	-	-	-	-
Clip-PanoFCN(Miao et al., 2022)	22.9	25.0	20.8	31.5	-	-	-	-
Video K-Net (Li et al., 2022)	26.1	-	-	31.5	-	-	-	-
TarVIS(Athar et al., 2023)	33.5	39.2	28.5	43.1	-	-	-	-
Tube-Link(Li et al., 2023c)	39.2	-	-	39.5	-	-	-	-
Video-kMax (Shin et al., 2024)	38.2	-	-	39.9	-	-	-	-
DVIS (Zhang et al., 2023a)	39.4	38.6	40.1	36.3	-	-	-	-
DVIS++ (Zhang et al., 2023b)	41.9	41.0	42.7	38.5	56.0	58.0	54.3	49.8
Ours	42.4	43.1	41.8	39.7	56.9	60.1	54.2	51.0
DVIS † (Zhang et al., 2023a)	43.2	43.6	42.8	42.8	-	-	-	-
DVIS++ † (Zhang et al., 2023b)	44.2	44.5	43.9	43.6	58.0	61.2	55.2	56.0
Ours †	45.3	47.5	43.4	45.3	58.5	63.1	54.5	56.1

significant performance gains. Particularly, context-aware instance features result in a notable +2.7 AP improvement over the baseline, a considerable increase compared to the +1.3 AP improvement observed with standard instance features. Further performance boosts are noted when PCC is introduced in experiments (iv- vi). The most substantial improvement is seen in experiment (vi), which records the highest performance of 29.5 AP by utilizing both \mathcal{L}_{CTX} and \mathcal{L}_{PCC} . This highlights the synergistic effect of integrating context-aware tracking with cross-frame contrastive loss, significantly enhancing the system’s accuracy and effectiveness.

In Tab. 3-(e), we evaluate the tracking network by initially using a fixed pre-trained segmentation network. Employing standard cross-attention with \hat{Q} achieved a high performance of 34.4 AP. Substituting this with our newly designed context-aware cross-attention further increases the performance by +1.7 AP, reaching 36.1 AP. These findings validate the efficacy of the context-aware feature, confirming its significant advantages for instance matching in complex video scenarios.

Context filter. Given that images feature objects at various scales, identifying the optimal receptive field size that functions effectively across different scenarios is essential. Our experiments, detailed in Tab. 3-(b), explore the effects of varying context filter sizes from 3 to 11. The optimal performance is achieved with a filter size of 9; larger sizes led to decreased performance, suggesting that excessively large receptive fields may detract from effective object matching by homogenizing the context features across all objects. Further investigation into different types of context filters shown in Tab. 3-(d) reveals that the average filter, which evenly reflects surrounding information, offers a well-defined benefit. In contrast, the learnable filter, which lacks specific directives on characterizing surrounding information, performs similarly to scenarios without enhanced context features, as demonstrated in Tab. 3-(a)-(v). This indicates the importance of a clearly defined context filter in improving the segmentation and tracking accuracy.

Table 3: Ablation studies on each component of CAVIS. (a-d) present the results from the segmentation network, while the others present those from the tracking network. “CL” denotes contrastive learning.

(a) Context-aware feature learning, PCC loss				(b) Context filter size		(c) Sampled frames	
CL with \hat{Q}	\mathcal{L}_{CTX}	\mathcal{L}_{PCC}	AP	Filter size	AP	# of frames	AP
(i)			26.4	3	27.3		
(ii)	✓		27.9	5	28.3	2	29.5
(iii)		✓	29.1	7	28.7	3	30.0
(iv)			27.6	9	29.5	4	28.7
(v)	✓		28.3	11	28.9		
(vi)		✓	29.5				

(d) Context filter type			(e) Cross-Attention for \mathcal{T}			(f) Context alignment		
Metric	Average	Learnable	Metric	\hat{Q}	Q	Metric	✗	✓
AP	29.5	28.4	AP	34.4	36.1	AP	32.8	36.1

The number of adjacent frames used during training. Our fundamental assumption is that the surrounding information between adjacent frames remains relatively stable, thereby aiding object matching. Tab. 3-(c) details the performance comparison based on the number of adjacent frames used during training. Utilizing three frames results in the highest performance, achieving 30.0 AP. Increasing the number of frames decreases performance, likely due to larger gaps between sampled frames which lead to more significant changes in the surrounding information, thus complicating object matching. Consequently, we have found that using three frames optimizes training effectiveness.

Context feature alignment. The tracking network aligns instance features and produces outputs in varying orders, necessitating the precise alignment of context features for accurate matching in subsequent frames. Misalignment of these features can lead to incorrect matching of context information for each object, significantly impacting performance. As demonstrated in Tab. 3-(f), misalignment results in a notable performance drop of 3.3 AP. This underscores the critical need for accurate alignment of context information to ensure robust object tracking performance.

6 CONCLUSION

In this paper, we introduce Context-Aware Video Instance Segmentation (CAVIS), a pioneering framework designed to enhance the accuracy and reliability of object tracking in complex video scenarios by integrating contextual information surrounding each instance. The introduction of the Context-Aware Instance Tracker (CAIT) and the innovative Prototypical Cross-frame Contrastive (PCC) loss are central to CAVIS’s effectiveness. CAIT leverages the surrounding context to enrich the core features of each instance, providing a more holistic view that significantly improves instance detection and segmentation under challenging conditions. Simultaneously, PCC loss ensures consistency of these enriched features across frames, reinforcing the temporal linkage between instances and enhancing the overall tracking robustness. Our experiments across multiple challenging benchmarks demonstrate that CAVIS significantly outperforms existing state-of-the-art methods, particularly excelling in scenarios that demand robust tracking capabilities. The integration of CAIT and PCC not only addresses the primary challenges of occlusions and motion but also effectively manages the presence of visually similar objects that can often mislead traditional VIS approaches.

ACKNOWLEDGMENTS

This work was supported by Korea Research Institute for defense Technology planning and advancement through Defense Innovation Vanguard Enterprise Project, funded by Defense Acquisition Program Administration(R230206), Institute of Information & Communications Technology Planning & Evaluation(IITP) grant funded by the Korea government(MSIT) (No.2014-3-00123, Development of High Performance Visual BigData Discovery Platform for Large-Scale Realtime Data Analysis) and the National Research Foundation of Korea (NRF) grant funded by the Korea government (MSIT) (No. RS-2023-00210908).

REFERENCES

- Ali Athar, Alexander Hermans, Jonathon Luiten, Deva Ramanan, and Bastian Leibe. Tarvis: A unified approach for target-based video segmentation. In *Proceedings of the IEEE/CVF Conference on Computer Vision and Pattern Recognition*, pp. 18738–18748, 2023.
- Moshe Bar. Visual objects in context. *Nature Reviews Neuroscience*, 5(8):617–629, 2004.
- Philipp Bergmann, Tim Meinhardt, and Laura Leal-Taixe. Tracking without bells and whistles. In *Proceedings of the IEEE/CVF international conference on computer vision*, pp. 941–951, 2019.
- Jiale Cao, Rao Muhammad Anwer, Hisham Cholakkal, Fahad Shahbaz Khan, Yanwei Pang, and Ling Shao. Sipmask: Spatial information preservation for fast image and video instance segmentation. In *Computer Vision–ECCV 2020: 16th European Conference, Glasgow, UK, August 23–28, 2020, Proceedings, Part XIV 16*, pp. 1–18. Springer, 2020.
- Nicolas Carion, Francisco Massa, Gabriel Synnaeve, Nicolas Usunier, Alexander Kirillov, and Sergey Zagoruyko. End-to-end object detection with transformers. In *European conference on computer vision*, pp. 213–229. Springer, 2020.
- Ting Chen, Simon Kornblith, Mohammad Norouzi, and Geoffrey Hinton. A simple framework for contrastive learning of visual representations. In *International conference on machine learning*, pp. 1597–1607. PMLR, 2020.
- Zhe Chen, Yuchen Duan, Wenhai Wang, Junjun He, Tong Lu, Jifeng Dai, and Yu Qiao. Vision transformer adapter for dense predictions. *arXiv preprint arXiv:2205.08534*, 2022.
- Bowen Cheng, Anwesa Choudhuri, Ishan Misra, Alexander Kirillov, Rohit Girdhar, and Alexander G Schwing. Mask2former for video instance segmentation. *arXiv preprint arXiv:2112.10764*, 2021a.
- Bowen Cheng, Alex Schwing, and Alexander Kirillov. Per-pixel classification is not all you need for semantic segmentation. *Advances in neural information processing systems*, 34:17864–17875, 2021b.
- Bowen Cheng, Ishan Misra, Alexander G Schwing, Alexander Kirillov, and Rohit Girdhar. Masked-attention mask transformer for universal image segmentation. In *Proceedings of the IEEE/CVF conference on computer vision and pattern recognition*, pp. 1290–1299, 2022.
- Ho Kei Cheng, Yu-Wing Tai, and Chi-Keung Tang. Rethinking space-time networks with improved memory coverage for efficient video object segmentation. *Advances in Neural Information Processing Systems*, 34:11781–11794, 2021c.
- Anwesa Choudhuri, Girish Chowdhary, and Alexander G. Schwing. Context-aware relative object queries to unify video instance and panoptic segmentation. In *Proceedings of the IEEE/CVF Conference on Computer Vision and Pattern Recognition (CVPR)*, pp. 6377–6386, June 2023.
- Alexey Dosovitskiy, Lucas Beyer, Alexander Kolesnikov, Dirk Weissenborn, Xiaohua Zhai, Thomas Unterthiner, Mostafa Dehghani, Matthias Minderer, Georg Heigold, Sylvain Gelly, Jakob Uszkoreit, and Neil Houlsby. An image is worth 16x16 words: Transformers for image recognition at scale. In *International Conference on Learning Representations*, 2021. URL <https://openreview.net/forum?id=YicbFdNTTy>.
- Su Ho Han, Sukjun Hwang, Seoung Wug Oh, Yeonchool Park, Hyunwoo Kim, Min-Jung Kim, and Seon Joo Kim. Visolo: Grid-based space-time aggregation for efficient online video instance segmentation. In *Proceedings of the IEEE/CVF Conference on Computer Vision and Pattern Recognition*, pp. 2896–2905, 2022.
- Kaiming He, Xiangyu Zhang, Shaoqing Ren, and Jian Sun. Deep residual learning for image recognition. In *Proceedings of the IEEE conference on computer vision and pattern recognition*, pp. 770–778, 2016.
- Kaiming He, Georgia Gkioxari, Piotr Dollár, and Ross Girshick. Mask r-cnn. In *Proceedings of the IEEE international conference on computer vision*, pp. 2961–2969, 2017.

-
- Miran Heo, Sukjun Hwang, Seoung Wug Oh, Joon-Young Lee, and Seon Joo Kim. Vita: Video instance segmentation via object token association. *Advances in Neural Information Processing Systems*, 35:23109–23120, 2022.
- Miran Heo, Sukjun Hwang, Jeongseok Hyun, Hanjung Kim, Seoung Wug Oh, Joon-Young Lee, and Seon Joo Kim. A generalized framework for video instance segmentation. In *Proceedings of the IEEE/CVF Conference on Computer Vision and Pattern Recognition*, pp. 14623–14632, 2023.
- De-An Huang, Zhiding Yu, and Anima Anandkumar. Minvis: A minimal video instance segmentation framework without video-based training. *Advances in Neural Information Processing Systems*, 35: 31265–31277, 2022.
- Sukjun Hwang, Miran Heo, Seoung Wug Oh, and Seon Joo Kim. Video instance segmentation using inter-frame communication transformers. *Advances in Neural Information Processing Systems*, 34: 13352–13363, 2021.
- Dahun Kim, Sanghyun Woo, Joon-Young Lee, and In So Kweon. Video panoptic segmentation. In *Proceedings of the IEEE/CVF Conference on Computer Vision and Pattern Recognition (CVPR)*, June 2020.
- Hojin Kim, Seunghun Lee, Hyeon Kang, and Sunghoon Im. Offline-to-online knowledge distillation for video instance segmentation. In *Proceedings of the IEEE/CVF Winter Conference on Applications of Computer Vision*, pp. 159–168, 2024.
- Harold W Kuhn. The hungarian method for the assignment problem. *Naval research logistics quarterly*, 2(1-2):83–97, 1955.
- Junlong Li, Bingyao Yu, Yongming Rao, Jie Zhou, and Jiwen Lu. Tcavis: Temporally consistent online video instance segmentation. In *Proceedings of the IEEE/CVF International Conference on Computer Vision*, pp. 1097–1107, 2023a.
- Minghan Li, Shuai Li, Wangmeng Xiang, and Lei Zhang. Mdqe: Mining discriminative query embeddings to segment occluded instances on challenging videos. In *Proceedings of the IEEE/CVF Conference on Computer Vision and Pattern Recognition*, pp. 10524–10533, 2023b.
- Xiangtai Li, Wenwei Zhang, Jiangmiao Pang, Kai Chen, Guangliang Cheng, Yunhai Tong, and Chen Change Loy. Video k-net: A simple, strong, and unified baseline for video segmentation. In *Proceedings of the IEEE/CVF Conference on Computer Vision and Pattern Recognition*, pp. 18847–18857, 2022.
- Xiangtai Li, Haobo Yuan, Wenwei Zhang, Guangliang Cheng, Jiangmiao Pang, and Chen Change Loy. Tube-link: A flexible cross tube framework for universal video segmentation. In *Proceedings of the IEEE/CVF International Conference on Computer Vision*, pp. 13923–13933, 2023c.
- Tsung-Yi Lin, Michael Maire, Serge Belongie, James Hays, Pietro Perona, Deva Ramanan, Piotr Dollár, and C Lawrence Zitnick. Microsoft coco: Common objects in context. In *Computer Vision—ECCV 2014: 13th European Conference, Zurich, Switzerland, September 6–12, 2014, Proceedings, Part V 13*, pp. 740–755. Springer, 2014.
- Ze Liu, Yutong Lin, Yue Cao, Han Hu, Yixuan Wei, Zheng Zhang, Stephen Lin, and Baining Guo. Swin transformer: Hierarchical vision transformer using shifted windows. In *Proceedings of the IEEE/CVF international conference on computer vision*, pp. 10012–10022, 2021.
- Ilya Loshchilov and Frank Hutter. Decoupled weight decay regularization. *arXiv preprint arXiv:1711.05101*, 2017.
- Jiaxu Miao, Yunchao Wei, Yu Wu, Chen Liang, Guangrui Li, and Yi Yang. Vspw: A large-scale dataset for video scene parsing in the wild. In *Proceedings of the IEEE/CVF Conference on Computer Vision and Pattern Recognition*, pp. 4133–4143, 2021.
- Jiaxu Miao, Xiaohan Wang, Yu Wu, Wei Li, Xu Zhang, Yunchao Wei, and Yi Yang. Large-scale video panoptic segmentation in the wild: A benchmark. In *Proceedings of the IEEE/CVF Conference on Computer Vision and Pattern Recognition*, pp. 21033–21043, 2022.

-
- Anton Milan, Laura Leal-Taixé, Ian Reid, Stefan Roth, and Konrad Schindler. Mot16: A benchmark for multi-object tracking. *arXiv preprint arXiv:1603.00831*, 2016.
- Seoung Wug Oh, Joon-Young Lee, Ning Xu, and Seon Joo Kim. Video object segmentation using space-time memory networks. In *Proceedings of the IEEE/CVF international conference on computer vision*, pp. 9226–9235, 2019.
- Aude Oliva and Antonio Torralba. The role of context in object recognition. *Trends in cognitive sciences*, 11(12):520–527, 2007.
- Maxime Oquab, Timothée Darcet, Théo Moutakanni, Huy Vo, Marc Szafraniec, Vasil Khalidov, Pierre Fernandez, Daniel Haziza, Francisco Massa, Alaaeldin El-Nouby, et al. Dinov2: Learning robust visual features without supervision. *arXiv preprint arXiv:2304.07193*, 2023.
- Jiyang Qi, Yan Gao, Yao Hu, Xinggang Wang, Xiaoyu Liu, Xiang Bai, Serge Belongie, Alan Yuille, Philip HS Torr, and Song Bai. Occluded video instance segmentation: A benchmark. *International Journal of Computer Vision*, 130(8):2022–2039, 2022.
- Siyuan Qiao, Yukun Zhu, Hartwig Adam, Alan Yuille, and Liang-Chieh Chen. Vip-deeplab: Learning visual perception with depth-aware video panoptic segmentation. In *Proceedings of the IEEE/CVF Conference on Computer Vision and Pattern Recognition*, pp. 3997–4008, 2021.
- Sarthak Sharma, Junaid Ahmed Ansari, J Krishna Murthy, and K Madhava Krishna. Beyond pixels: Leveraging geometry and shape cues for online multi-object tracking. In *2018 IEEE International Conference on Robotics and Automation (ICRA)*, pp. 3508–3515. IEEE, 2018.
- Inkyu Shin, Dahun Kim, Qihang Yu, Jun Xie, Hong-Seok Kim, Bradley Green, In So Kweon, Kuk-Jin Yoon, and Liang-Chieh Chen. Video-kmax: A simple unified approach for online and near-online video panoptic segmentation. In *Proceedings of the IEEE/CVF Winter Conference on Applications of Computer Vision*, pp. 229–239, 2024.
- Siyu Tang, Mykhaylo Andriluka, Bjoern Andres, and Bernt Schiele. Multiple people tracking by lifted multicut and person re-identification. In *Proceedings of the IEEE conference on computer vision and pattern recognition*, pp. 3539–3548, 2017.
- Laurens Van der Maaten and Geoffrey Hinton. Visualizing data using t-sne. *Journal of machine learning research*, 9(11), 2008.
- Yuqing Wang, Zhaoliang Xu, Xinlong Wang, Chunhua Shen, Baoshan Cheng, Hao Shen, and Huaxia Xia. End-to-end video instance segmentation with transformers. In *Proceedings of the IEEE/CVF conference on computer vision and pattern recognition*, pp. 8741–8750, 2021.
- Sanghyun Woo, Dahun Kim, Joon-Young Lee, and In So Kweon. Learning to associate every segment for video panoptic segmentation. In *Proceedings of the IEEE/CVF Conference on Computer Vision and Pattern Recognition*, pp. 2705–2714, 2021.
- Jialian Wu, Sudhir Yarram, Hui Liang, Tian Lan, Junsong Yuan, Jayan Eledath, and Gerard Medioni. Efficient video instance segmentation via tracklet query and proposal. In *Proceedings of the IEEE/CVF Conference on Computer Vision and Pattern Recognition*, pp. 959–968, 2022a.
- Junfeng Wu, Yi Jiang, Song Bai, Wenqing Zhang, and Xiang Bai. Seqformer: Sequential transformer for video instance segmentation. In *European Conference on Computer Vision*, pp. 553–569. Springer, 2022b.
- Junfeng Wu, Qihao Liu, Yi Jiang, Song Bai, Alan Yuille, and Xiang Bai. In defense of online models for video instance segmentation. In *European Conference on Computer Vision*, pp. 588–605. Springer, 2022c.
- Jiarui Xu, Yue Cao, Zheng Zhang, and Han Hu. Spatial-temporal relation networks for multi-object tracking. In *Proceedings of the IEEE/CVF international conference on computer vision*, pp. 3988–3998, 2019.

-
- Ning Xu, Linjie Yang, Yuchen Fan, Dingcheng Yue, Yuchen Liang, Jianchao Yang, and Thomas Huang. Youtube-vos: A large-scale video object segmentation benchmark. *arXiv preprint arXiv:1809.03327*, 2018.
- Linjie Yang, Yuchen Fan, and Ning Xu. Video instance segmentation. In *Proceedings of the IEEE/CVF International Conference on Computer Vision*, pp. 5188–5197, 2019.
- Linjie Yang, Yuchen Fan, Yang Fu, and Ning Xu. The 3rd large-scale video object segmentation challenge - video instance segmentation track, June 2021a.
- Shusheng Yang, Yuxin Fang, Xinggang Wang, Yu Li, Chen Fang, Ying Shan, Bin Feng, and Wenyu Liu. Crossover learning for fast online video instance segmentation. In *Proceedings of the IEEE/CVF International Conference on Computer Vision*, pp. 8043–8052, 2021b.
- Shusheng Yang, Xinggang Wang, Yu Li, Yuxin Fang, Jiemin Fang, Wenyu Liu, Xun Zhao, and Ying Shan. Temporally efficient vision transformer for video instance segmentation. In *Proceedings of the IEEE/CVF conference on computer vision and pattern recognition*, pp. 2885–2895, 2022.
- Kaining Ying, Qing Zhong, Weian Mao, Zhenhua Wang, Hao Chen, Lin Yuanbo Wu, Yifan Liu, Chengxiang Fan, Yunzhi Zhuge, and Chunhua Shen. Ctvis: Consistent training for online video instance segmentation. In *Proceedings of the IEEE/CVF International Conference on Computer Vision*, pp. 899–908, 2023.
- Ye Yu, Jialin Yuan, Gaurav Mittal, Li Fuxin, and Mei Chen. Batman: Bilateral attention transformer in motion-appearance neighboring space for video object segmentation. In *European Conference on Computer Vision*, pp. 612–629. Springer, 2022.
- Tao Zhang, Xingye Tian, Yu Wu, Shunping Ji, Xuebo Wang, Yuan Zhang, and Pengfei Wan. Dvis: Decoupled video instance segmentation framework. *arXiv preprint arXiv:2306.03413*, 2023a.
- Tao Zhang, Xingye Tian, Yikang Zhou, Shunping Ji, Xuebo Wang, Xin Tao, Yuan Zhang, Pengfei Wan, Zhongyuan Wang, and Yu Wu. Dvis++: Improved decoupled framework for universal video segmentation. *arXiv preprint arXiv:2312.13305*, 2023b.
- Yifu Zhang, Chunyu Wang, Xinggang Wang, Wenjun Zeng, and Wenyu Liu. Fairmot: On the fairness of detection and re-identification in multiple object tracking. *International Journal of Computer Vision*, 129:3069–3087, 2021.
- Xingyi Zhou, Vladlen Koltun, and Philipp Krähenbühl. Tracking objects as points. In *European conference on computer vision*, pp. 474–490. Springer, 2020.
- Xizhou Zhu, Weijie Su, Lewei Lu, Bin Li, Xiaogang Wang, and Jifeng Dai. Deformable detr: Deformable transformers for end-to-end object detection. *arXiv preprint arXiv:2010.04159*, 2020.

A APPENDIX

A.1 LIMITATION

Video Instance Segmentation (VIS) is an advanced technology designed to perform segmentation and tracking concurrently, capturing the trajectories of individual instances within a video. While this technology has significant benefits, it also poses potential risks if misused, particularly in surveillance applications. Such misuse could lead to severe privacy infringements. It is important to note, however, that the dataset used in this study is a standard one within the VIS community and does not include any sensitive or personal information. This precaution helps mitigate the risk of our trained model being used for harmful purposes. Nonetheless, the potential for negative impacts should not be underestimated, and ethical considerations must guide the deployment of VIS technologies.

A.2 EXPERIMENTAL DETAILS

A.2.1 DATASETS

Youtube-VIS 2019 and 2021 YouTube-VIS was introduced by Yang et al. in their pioneering study on the VIS task (Yang et al., 2019). This dataset comprises high-resolution YouTube videos, categorized into 40 distinct classes. The 2019 version of the dataset includes 2,238 videos for training, 302 for validation, and 343 for testing (Yang et al., 2019). The 2021 update expands these numbers to 2,985, 421, and 453 videos for training, validation, and testing, respectively (Yang et al., 2021a). YouTube-VIS is utilized across various pixel-level video understanding tasks, including VIS, video semantic segmentation, and video object detection.

OVIS The OVIS dataset (Qi et al., 2022) presents a significant challenge with its frequent occlusions and a realistic representation of common everyday objects. This makes it highly relevant for real-world applications. OVIS videos are longer and contain more objects compared to those in YouTube-VIS, which increases the complexity of segmentation and tracking tasks. The dataset is organized into training, validation, and test sets, with 607, 140, and 154 videos, respectively.

VIPSeg VIPSeg (Miao et al., 2022) is a comprehensive Video Panoptic Segmentation dataset that includes 3,536 videos and 84,750 frames, annotated with pixel-level panoptic labels. Unlike earlier VPS datasets that primarily focus on street views, VIPSeg offers a broader range of challenges and practical scenarios. It features 232 diverse settings and is annotated with 58 ‘thing’ classes and 66 ‘stuff’ classes, making it one of the most diverse and challenging datasets available in the field.

A.2.2 IMPLEMENTATION

Our segmentation approach employs the Mask2Former architecture (Cheng et al., 2022), utilizing the officially recommended hyperparameters. For all experimental settings, we follow established practices by incorporating COCO joint training, as adopted in previous methodologies (Wu et al., 2022b; Heo et al., 2022; 2023; Ying et al., 2023; Zhang et al., 2023a). The tracking network consists of six transformer blocks. Within the tracking network’s transformer blocks, we innovate by replacing the standard cross-attention layer with the referring cross-attention layer, as introduced in (Zhang et al., 2023a). Additionally, we conduct experiments with the temporal refiner (Zhang et al., 2023a) over 160k iterations, specifically analyzing sequences of 15 consecutive frames to enhance tracking accuracy.

For efficient training, we adopt a staged approach where the segmentation network is trained first, followed by the tracking network with all other parameters frozen, promoting stability and efficiency in learning, as suggested by previous studies (Zhang et al., 2023a; Li et al., 2023a). Optimization is carried out using the AdamW optimizer (Loshchilov & Hutter, 2017), with a starting learning rate of $1e-4$ and a weight decay of $5e-2$. The training process spans 40k iterations for the segmentation network and 160k iterations for the tracking network, with learning rate reductions scheduled at 28k and 112k iterations, respectively. During training, we sample three frames for the segmentation network and five frames for the tracking network from each of eight batched videos. These frames undergo resizing to ensure the shorter side is between 320 and 640 pixels, while the longer side does not exceed 768 pixels. The loss function weights are set to $\lambda_{cls} = 2.0$, $\lambda_{bce} = 5.0$, $\lambda_{dice} = 5.0$, $\lambda_{ctx} = 2.0$, and $\lambda_{pro} = 2.0$ to balance the contributions of each component during training. For inference, the

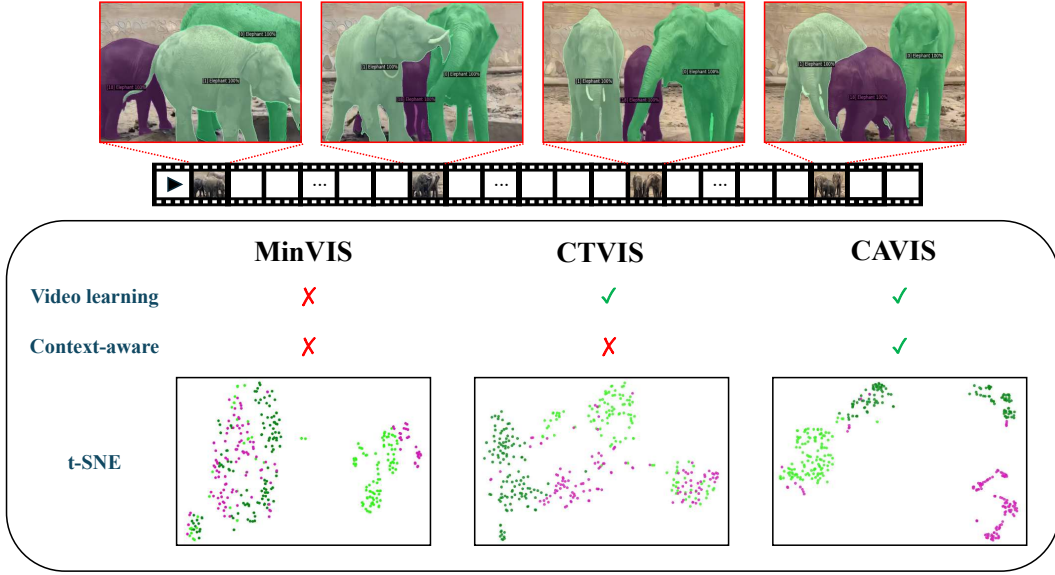


Figure 4: Visualization of object embeddings. Each point on the t-SNE (Van der Maaten & Hinton, 2008) plot represents the learned object embeddings. The three different colors of points indicate the embeddings of three different elephants throughout the entire video.

shorter side of input frames is scaled down to 448 pixels to maintain a consistent aspect ratio across inputs. All experiments are conducted using 8 RTX2080Ti GPUs for the ResNet-50 backbone and 8 RTX3090 GPUs for the Swin-L and ViT-L backbones, ensuring adequate computational resources are available for the demands of each model configuration.

A.3 ADDITIONAL EXPERIMENTS

Analysis on object embeddings. To demonstrate the effectiveness of our context-aware instance learning, we compare the distribution of object embeddings from three different models, as shown in Fig. 4. MinVIS does not engage in video learning, resulting in less effective distinction between objects. Compared to MinVIS, CTVIS shows a clearer object distinction by employing contrastive learning among object embeddings, but it still exhibits some overlaps in object clusters. In contrast, CAVIS forms much more distinct object clusters, highlighting the advantage of leveraging contextual information for object identification.

Qualitative results. We provide additional qualitative results of CAVIS across various datasets, as depicted in Fig. 5-8. These results underscore the robust capability of CAVIS to track objects in diverse scenarios for both VIS and VPS tasks. Notably, CAVIS excels in environments featuring numerous similar objects, fast-moving objects, and significant occlusions, demonstrating its effectiveness across complex dynamic scenes.

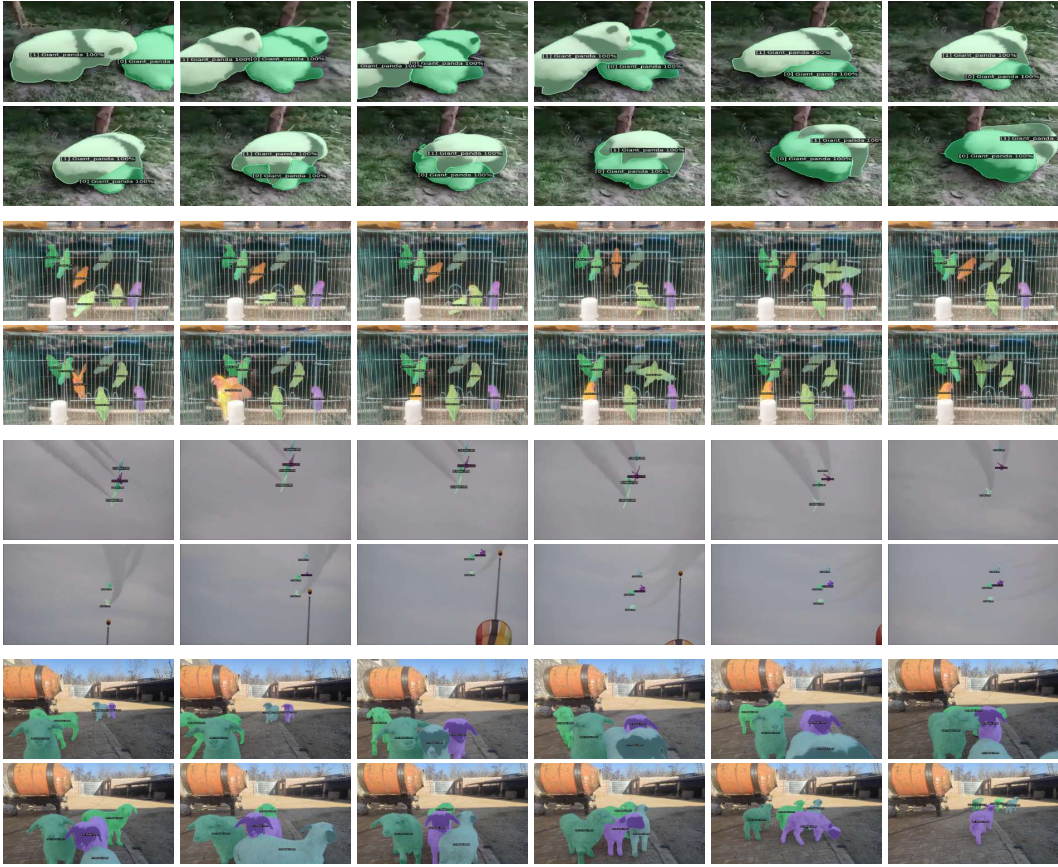


Figure 5: Additional qualitative results on OVIS dataset.

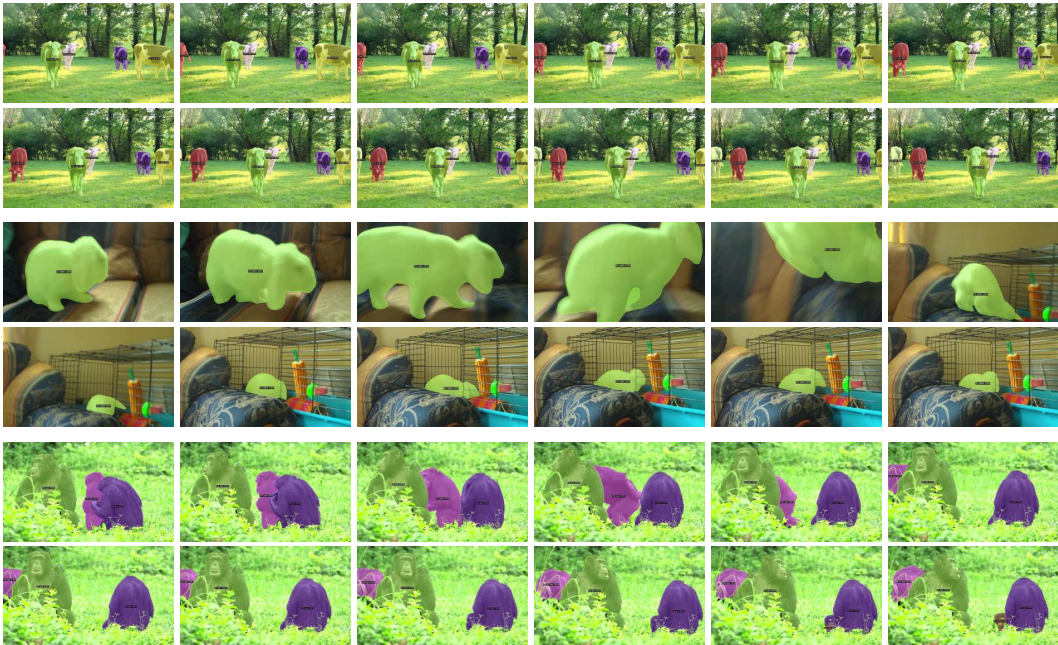


Figure 6: Additional qualitative results on Youtube-VIS 2019 dataset.



Figure 7: Additional qualitative results on Youtube-VIS 2021 dataset.



Figure 8: Additional qualitative results on VIPSeg dataset.